ACS APPLIED ENERGY MATERIALS

www.acsaem.org Article

# Influence of Structural Distortion and Lattice Dynamics on Li-Ion Diffusion in $Li_3OCl_{1-x}Br_x$ Superionic Conductors

Ronghan Chen, Zhenming Xu, Yuechuan Lin, Buyao Lv, Shou-Hang Bo, and Hong Zhu*

Cite This: https://dx.doi.org/10.1021/acsaem.0c02519 Read Online

ACCESS | Metrics & More | Article Recommendations | Supporting Information

**ABSTRACT:** The antiperovskite superionic conductors $Li_3OCl$ and $Li_3OBr$ show great differences in ionic conductivity. The more polarizable $Li_3OBr$ shows a lower ionic conductivity than $Li_3OCl$, contradicting the idea that a more polarizable framework is beneficial for ionic conduction. In this work, we study the influence of substituting Cl with Br on the local structure, lattice dynamics, and Li-ion conductivity of $Li_3OCl_{1-x}Br_x$, based on first-principles calculations. We find that the incorporation of Br does soften the overall lattice stiffness of $Li_3OCl_{1-x}Br_x$, but the accompanying local structural distortion plays a dominant role in changing the activation energy for Li-ion diffusion, which could increase the site energy as well as the Li-ion vibration frequency. We suggest that more distorted initial octahedral sites and less distorted saddle trigonal-plane sites can lead to better ionic transport. In addition, the correlation between activation energy and the pre-exponential factor of diffusivity extracted from the Arrhenius plot of $Li_3OCl_{1-x}Br_x$ is found to be nonlinear, which is due to the decreasing migration entropy with increasing activation energy.

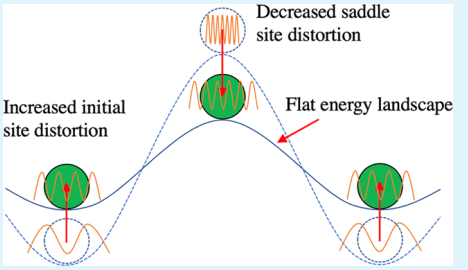


**KEYWORDS:** *ionic conductor, antiperovskite, diffusion, distortion, lattice dynamics*



## 1. INTRODUCTION

Lithium-ion batteries have been widely used in portable electronic devices and are now developed for large-scale applications. However, lithium batteries with liquid electrolytes have safety issues including flammability, leakage, and low chemical stability.[1] All-solid-state lithium-ion batteries based on solid electrolytes not only exhibit excellent safety performance but also have high energy density owing to the usage of a high-capacity electrode such as a Li metal anode.[2,3] A good solid electrolyte should have high ionic conductivity, wide electrochemical stability window, good chemical compatibility with electrodes, and low cost.[4,5] But one specific electrolyte can hardly meet all of the requirements simultaneously.[6] Understanding ionic diffusion in solid electrolytes can guide the design of high-performance ionic conductors.[7,8]

The lithium-rich antiperovskites $Li_3OX$ (X = Cl, Br or a mixture of halides) have attracted interest since Zhao et al.[9] reported the mixed halide $Li_3OCl_{0.5}Br_{0.5}$ with high ionic conductivity of $1.94 \times 10^{-3}$ S $cm^{-1}$ at room temperature. However, following studies have shown that the two endmembers, i.e., $Li_3OCl$ and $Li_3OBr$, possess much lower ionic conductivity.[10,11] The interesting phenomenon is that $Li_3OBr$, even though with more polarizable anion Br, shows lower ionic conductivity than $Li_3OCl$. First-principles calculations by Emly et al.[12] showed that the activation energy barrier for a charged Li vacancy in $Li_3OBr$ is 370 meV while it is only 310 meV in $Li_3OCl$. This contradicts the idea that a more polarizable anion framework can induce a softer lattice and thus lower the activation barrier.[13−15] Furthermore, the composition with the highest conductivity is not the two endmembers but the mixed halide compound. Deng et al.[16] studied $Li_3OCl_{1-x}Br_x$ by first-principles calculations and found that Cl ions along the migration channel can decrease the lithium migration barrier. Using percolation theory, they predicted that $Li_3OCl_{1-x}Br_x$ with $0.235 \leq x \leq 0.395$ would have higher ionic conductivity. Kim et al.[17] extended the study to 24 different antiperovskites, namely, $X_3AB$ (X = Li or Na, and A = O, S or Se, and B = F, Cl, Br, or I). They used tolerance factor, *t*, to describe the degree of lattice distortion, where the smaller tolerance factor stands for larger distortions. They found that the smaller tolerance factor corresponds to the lower activation energy barrier. However, the tolerance factor can hardly extend to other materials to characterize the structure appropriately and cannot explain the outstanding performance of a mixed halide compound. Hence, the investigation on the influences of the local structure and lattice dynamics on ionic conductivity can provide insights into universal descriptors to find advanced solid electrolytes.

In this study, we perform a comprehensive investigation of the correlated influences of structural distortion and lattice

Received: October 12, 2020
Accepted: February 2, 2021

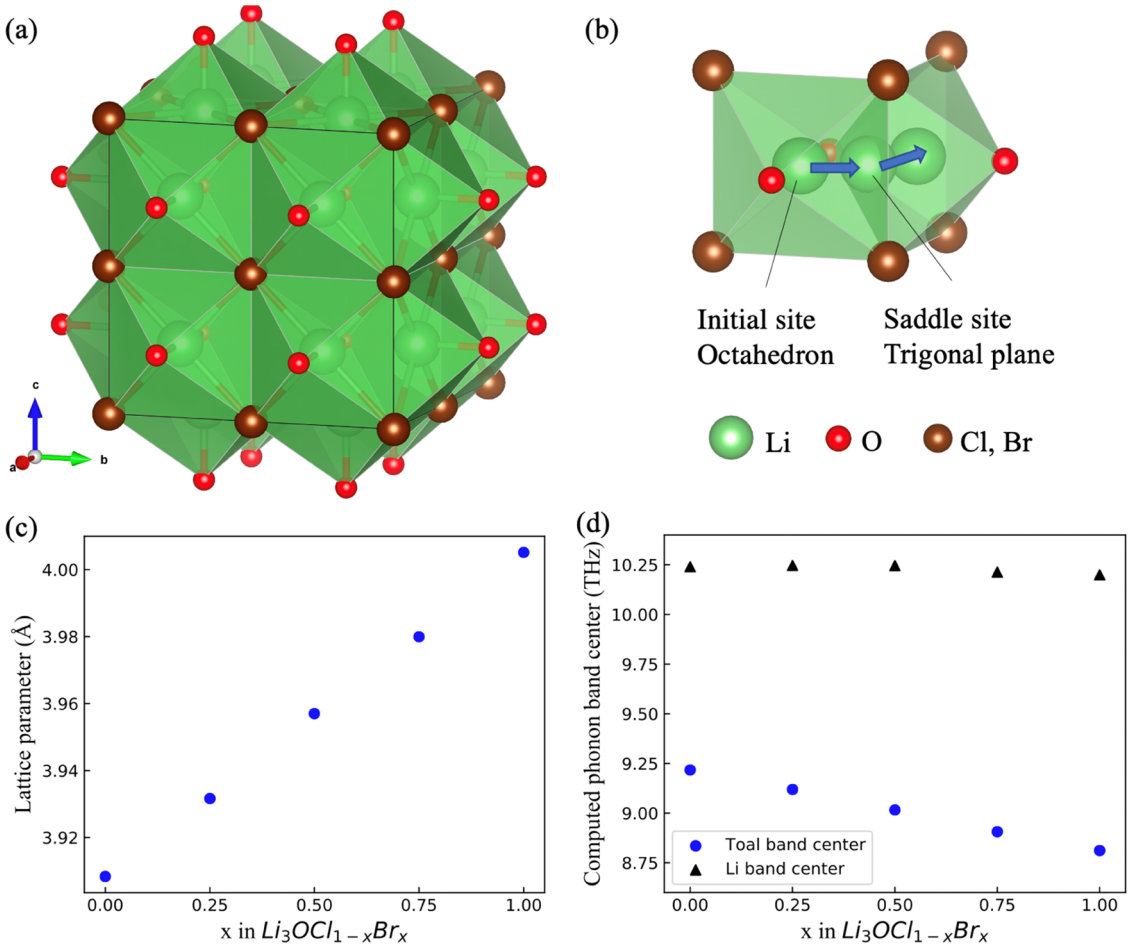


**Figure 1.** (a) Crystal structure of 2 × 2 × 2 $Li_3OCl_{1-x}Br_x$. (b) Li-ion migration pathway between two adjacent octahedrons through a trigonal plane. (c) Lattice parameter of $Li_3OCl_{1-x}Br_x$, increasing with the Br concentration. (d) Calculated total and Li-projected phonon band centers.

dynamics on the Li-ion diffusivity in $Li_3OCl_{1-x}Br_x$ by first-principles calculations based on transition-state theory. First-principles simulations can offer fundamental insights into ion transport mechanisms in superionic conductors at the atomistic scale and promote the design of solid electrolytes.[18,19] Using a combination of the nudged elastic band method, continuous symmetry measure, and phonon calculations, we monitor the mobile-ion behavior during the migration process in every possible pathway. The total phonon density of state affirms that the replacement of Cl with Br truly causes a softer lattice framework. However, the vibration frequency of the mobile Li ion does not simply decrease with the addition of Br. The ionic radius difference of Cl and Br distorts the local structure of the mobile Li ion. At the initial site, the distorted environment can increase its site energy. At the saddle site, the distorted environment will block the Li-ion hopping. Hence, we deduce that more distorted initial sites and less distorted saddle sites are favorable to obtain low activation energy. In addition, we investigate the correlation between the pre-exponential factor and activation energy both obtained from the Arrhenius plot. The correlation is further explained by calculating the governed parameters in the prefactor.

## 2. COMPUTATIONAL METHODOLOGY

The density functional theory (DFT) calculations were carried out within the Vienna Ab initio Simulation Package (VASP).[20] The ion−electron interactions were modeled by the projector augmented wave (PAW)[21] method. The generalized gradient approximation (GGA) with the Perdew−Burke−Ernzerhof (PBE)[22] functional was adopted to consider the electron exchange-correlation energy.

In this work, 2 × 2 × 2 $Li_3OCl_{1-x}Br_x$ supercells with $x$ = 0, 0.25, 0.5, 0.75, and 1 were built and relaxed for the subsequent calculations. A plane-wave energy cutoff of 520 eV was used and the Brillouin zone was sampled by a 3 × 3 × 3 Γ-centered $k$-mesh. The convergence criteria for structural optimization were 0.01 eV $Å^{-1}$ in force and $10^{-5}$ eV in energy. Phonon density of states (DOS) calculations were carried out based on the density functional perturbation theory (DFPT),[23] as implemented in the PHONOPY code.[24]

The phonon band center, or average vibrational frequency $\omega_{av}$, is defined as

$$\omega_{av} = \frac{\int \omega \mathrm{DOS}(\omega) \mathrm{d}\omega}{\int \mathrm{DOS}(\omega) \mathrm{d}\omega} \quad (1)$$

The Li vacancy migration barriers in 2 × 2 × 2 $Li_3OCl_{1-x}Br_x$ supercells with one compensating background charge were obtained using the climbing image nudged elastic band (CINEB)[25] method. Ab initio molecular dynamics (AIMD) simulations were performed to evaluate charged Li vacancy diffusivity. For the sake of computational efficiency, a smaller plane-wave energy cutoff of 400 eV was selected for AIMD simulations with a 1 × 1 × 1 Γ-centered $k$-mesh. All supercell


https://dx.doi.org/10.1021/acsaem.0c02519
ACS Appl. Energy Mater. XXXX, XXX, XXX−XXX

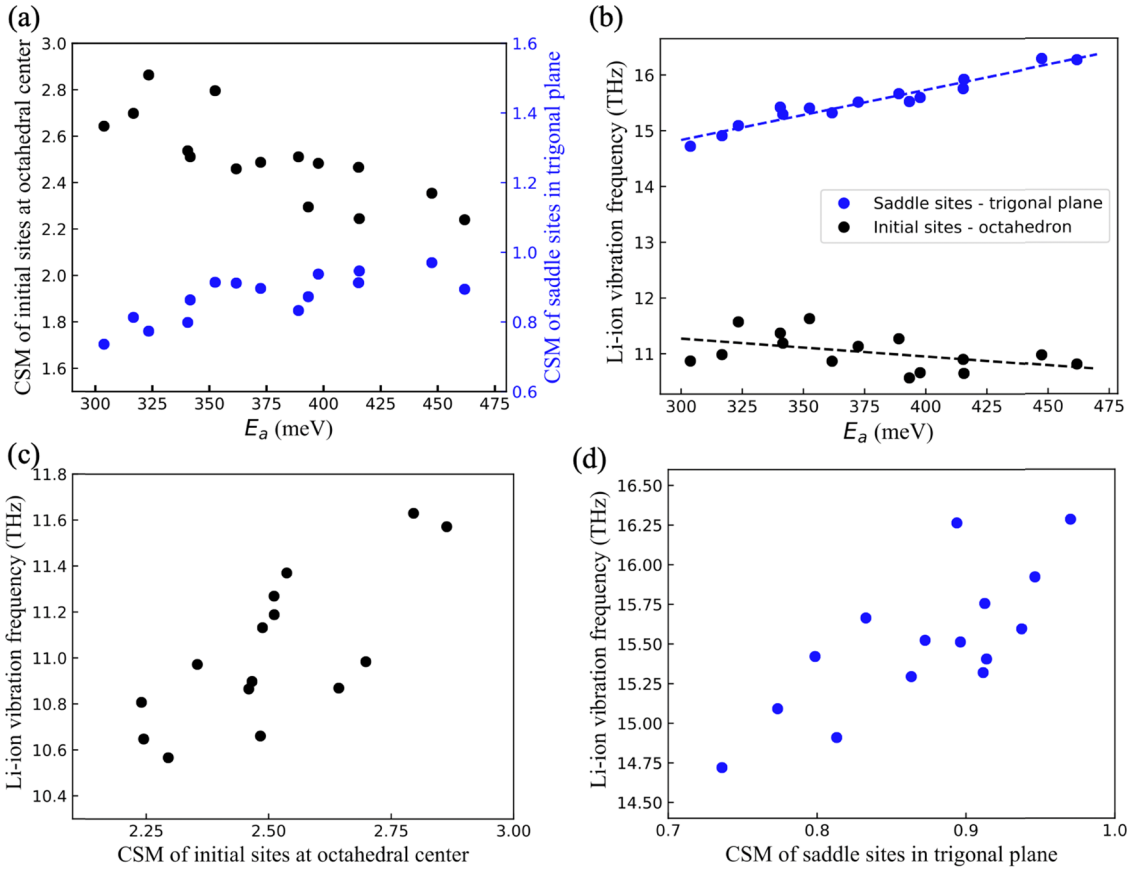


**Figure 2.** (a) Correlation between site distortions and activation energy. (b) Correlation between mobile Li-ion vibration frequency and activation energy. (c, d) Correlation between mobile Li-ion vibration frequency and distortions of initial sites and saddle sites.

systems were simulated for 60 000 steps with a time step of 2 fs and a total time of 240 ps in the NVT ensemble using a Nosé–Hoover thermostat.[26,27]

The mean square displacement (MSD) is calculated as

$$\langle[\vec{r}(t)]^2\rangle = \frac{1}{N}\sum_i \langle[\vec{r}_i(t+t_0) - \vec{r}_i(t_0)]^2\rangle \quad (2)$$

where $\vec{r}_i(t)$ is the vector of instantaneous coordinates of the $i$th Li ion and $N$ is the number of the mobile Li ion in the cell. The Li diffusion coefficient is obtained via a linear fit of MSD with time as described by the Einstein relation.

$$D = \frac{1}{t}\langle[\vec{r}_i(t)]^2\rangle \quad (3)$$

The diffusion coefficient and temperature satisfy the Arrhenius relationship

$$D = D_0 \exp\left(-\frac{E_a}{k_B T}\right) \quad (4)$$

where $k$ is the Boltzmann constant and $T$ is the temperature in K. The Arrhenius plot was constructed from simulations at multiple temperatures (1150–1900 K) to obtain the activation energy $E_a$ and prefactor $D_0$.

## 3. RESULTS AND DISCUSSION

**3.1. Influence of Structural Changes.** The crystal structure and the Li vacancy migration path of the antiperovskites $Li_3OCl_{1-x}Br_x$ ($x$ = 0, 0.25, 0.5, 0.75, 1) are illustrated in Figure 1a,b. The initial and final lithium sites are both octahedral sites, while the saddle point of the migration path is in a trigonal plane. Even though Emly et al.[12] reported a Li interstitial dumbbell migration mechanism with lower activation energy than the vacancy mechanism, the Li interstitial defects have higher formation energy. Wu et al.[28] studied the transport mechanisms and concluded that the Li vacancy is the dominant charge carrier while the Li interstitial might facilitate Li-ion transport. In addition, the variation of activation energy with halide pair arrangement is similar in these two mechanisms.[12,16] Therefore, in this work, we focus on the single Li vacancy migration in the antiperovskites $Li_3OCl_{1-x}Br_x$. The structures of the two endmembers, $Li_3OCl$ and $Li_3OBr$, are unique. However, for the mixed anion compositions ($x$ = 0.25, 0.5, and 0.75), the halide anion may arrange in different ways and even form a disordered anion halide sublattice.[12] Because all of the ordering of halide ions in each composition have been reported to have similar formation energies,[16] to simplify the study, we mainly focused on the structures with highest symmetry (Figure S1 and Table S1) for the following calculations in this work. As shown in Figure 1c, with increasing Br content, the lattice parameters increase linearly as a result of the larger anion radius, obeying Vegard's law.

Since different halide pairs lead to various migration environments, a number of 15 different migration pathways exist in these five $Li_3OCl_{1-x}Br_x$ compounds. To take a closer look at the structural influences on the Li-ion diffusion, we studied the local environment of each migration pathway. In light of superionic nature, the migration enthalpy is taken as


https://dx.doi.org/10.1021/acsaem.0c02519
ACS Appl. Energy Mater. XXXX, XXX, XXX–XXX

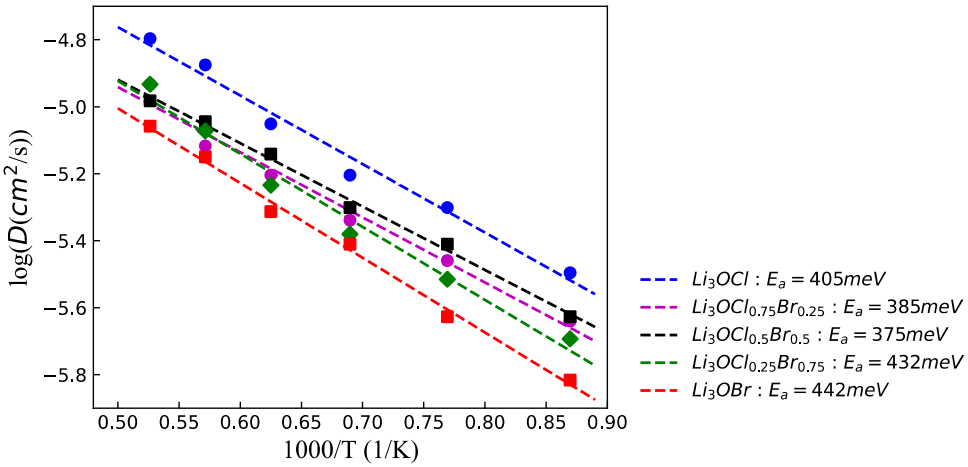


**Figure 3.** Arrhenius plot of the Li-ion diffusion coefficients in $Li_3OCl_{1-x}Br_x$ ($x$ = 0, 0.25, 0.5, 0.75, 1) from AIMD simulations at different temperatures.

activation energy by neglecting the defect formation enthalpy. The activation energies, corresponding migration pathways, and bond information are listed in Tables S2 and S3.

Inspired by the effect of a distorted local structure on ion diffusion,[17,29] we analyzed the site distortions of $Li_3OCl_{1-x}Br_x$ using the continuous symmetry measures (CSM).[30,31] The CSM indicates the distortion of the coordination environment with respect to a perfect polyhedron. A larger CSM value means the local environment is more distorted. Figure 2a shows the relationship between the site distortions and the activation energy. With increasing CSM of the initial sites and decreasing CSM of the saddle sites, the activation energy becomes lower. Distorted initial sites tend to increase the system energy, activating the initial site for ion diffusion.[32] On the other hand, distorted saddle sites constrict the conduction pathway and hinder the ionic transport.[33] Therefore, more distorted initial sites and less distorted saddle sites together flatten the energy landscape of $Li_3OCl_{1-x}Br_x$.

Our finding is corroborated by several experimental observations. Hautier's group[29] attributed the low activation energy and outstanding ionic conductivity in $LiTi_2(PS_4)_3$ to the highly distorted Li-ion sites. They claimed the distortions make the ground state unstable and lead to a smooth energy landscape. A similar phenomenon can be found in $Na_9(AlS_4)$-$(SiS_4)$.[34] However, the condition in which distortions have a negative influence on ionic conductivity is also reported. Stoldt et al.[33] found that in NASICON-type $LiGe_{2-x}Sn_x(PO_4)_3$ and $Li_{1+x}Al_xGe_{2-y-(1/2)x}Sn_{y-(1/2)x}(PO_4)_3$, bottleneck regions suffer distortion due to large radius disparity between cations and therefore the Li-ion transport is constricted. Our finding specifies the opposite preference for distortion in initial and saddle sites with the help of CSM as a descriptor.

**3.2. Influence of Lattice Dynamics.** Previous studies have suggested that the introduction of a more polarizable anion contributes to a soft lattice and thereby lower activation energy.[13,14,35,36] Here, the effect of lattice dynamics in $Li_3OCl_{1-x}Br_x$ is studied based on phonon calculations. The dynamic stabilities of the five compounds are verified by the phonon calculations (the phonon DOS can be found in Figure S2). Both the calculated total and Li-projected phonon band centers are shown in Figure 1d. With increasing Br content, the total phonon band center becomes lower due to its polarizability. Interestingly, the Li-projected phonon band center varies little. This indicates that even though the introduction of a more polarizable anion truly softens the lattice, the overall interaction between the mobile Li ion and anions does not weaken obviously. Therefore, the variation of the local Coulombic interactions surrounding the mobile lithium ions and its effect on the activation energy need more studies.[37]

As the vibration modes of hopping Li ion during migration can better describe the local lattice vibration,[35] they were calculated for each migration pathway as shown in Figure 2b. The Li-ion vibration frequency in Figure 2b is captured during the migration process, i.e., when the hopping Li ion is at the initial site and saddle site separately. We capture the hopping Li ion and fix other atoms.[38,39] With a decreasing activation energy, the vibration frequency of the Li ion is increasing at the initial site while decreasing at the saddle site. We note that the Li-ion vibration frequency as well as its variation at saddle sites is larger than those at initial sites due to the more constrained local environment of saddle sites (trigonal plane) than initial sites (octahedron) in $Li_3OCl_{1-x}Br_x$.

We find that the overlap between Li-projected and anion-projected phonon DOS gradually decreases as the Br content increases (Figure S3). The overlap of the Li ion and anion vibration implies that a part of the Li ion may hop at the same time-scale with the anion motion.[40] The vibration of the anion may transfer momentum to the Li ion and assist the Li ion to hop to another site.[41] The incorporation of larger Br in $Li_3OCl_{1-x}Br_x$ may lead to a larger moment of inertia and thereby hinder the rotation motion effect as found in other material systems.[42] Further work is needed to reveal the proportion of this coupled motion contributing to the overall ionic conductivity.

**3.3. Correlation between Lattice Dynamics and Structural Distortion.** Both the lattice dynamics and static structure can affect the ionic transport property.[43] Generally, the incorporation of a larger and more polarizable anion can decrease the activation energy barrier. Meanwhile, more distorted initial sites and less distorted saddle sites can flatten the energy landscape, as discussed above. However, the incorporation of more polarizable anion may lead to an unfavorable structural change and hence offset the improvement on activation energy.[44] Herein, the convoluted relationship between structural distortion and cation vibration is


https://dx.doi.org/10.1021/acsaem.0c02519
ACS Appl. Energy Mater. XXXX, XXX, XXX−XXX

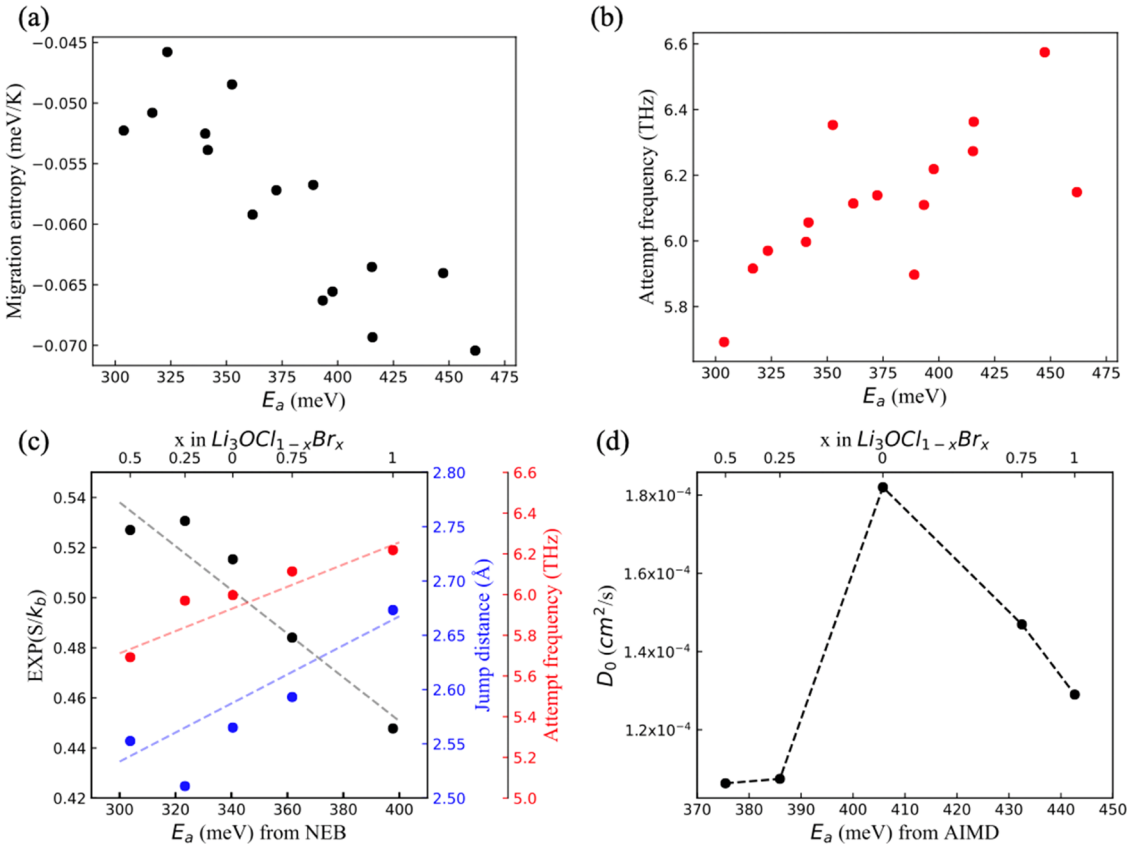


**Figure 4.** (a) Calculated migration entropy using the Vineyard method, only the frequency of the hopping Li ion was considered. (b) True attempt frequency of the hopping Li ion calculated from the jump distance and activation energy. (c) With increasing activation energy, the jump distance and attempt frequency increase while the migration entropy decreases, leading to an optimal combination and maximum prefactor $D_0$ at the middle. (d) Correlation between prefactor $D_0$ and activation energy extracted from $D = D_0 \exp\left(\frac{\Delta E_a}{kT}\right)$ by AIMD. Dashed lines are a guide to the eyes only.

shown in Figure 2c,d. With increasing site distortion, the local vibration frequency of hopping Li ion increases, indicating that the structural distortion can alter the Li-ion vibration properties.

To explore the overall influence of mixed halide, the AIMD simulations were performed. The MSD-$\Delta t$ plots shown in Figure S4 exhibit a good linear relationship. Figure 3 shows the Arrhenius plot for various Li-ion diffusion coefficients at elevated temperatures.[45] $Li_3OCl$, even with a stiffer lattice framework, has lower activation energy than $Li_3OBr$. The more distorted initial sites and less distorted saddle sites in $Li_3OCl$ should contribute to the lower activation energy compared with $Li_3OBr$. The mixed $Li_3OCl_{0.5}Br_{0.5}$ makes the most benefit of structural distortion and hence has the lowest activation energy compared to two endmembers. This corroborates that in $Li_3OCl_{1-x}Br_x$, the influence of local structural distortion is dominant. The conclusion should hold regardless of the selection of a disordered anion halide sublattice (see the details in the Supporting Information).

**3.4. Migration Entropy and Meyer−Neldel Rule.** The significance of pre-exponential factor $D_0$ seems to be overlooked and efforts are mainly made on reducing the activation barrier. There exists an empirical relationship that decreasing activation energy is accompanied by a decreasing pre-exponential factor, also known as the Meyer−Neldel rule.[46−48] This correlation can be applied to both the prefactor of diffusivity $D_0$ and the prefactor of conductivity $\sigma_0$.[49,50] These two terms are connected by the Nernst−Einstein equation $\sigma_0 = \frac{Nq^2}{VkT} D_0$ assuming dilute and isolated mobile-ion carriers.[51] However, the Meyer−Neldel rule is not valid for some families of solid electrolytes.[52−55] For instance, in $Li_6PS_5X$ (X = Cl, Br, and I), when the disorder vanishes, increasing prefactor with increasing activation energy cannot be observed.[13] Recently, Hautier and co-workers reported $LiTi_2(PS_4)_3$ with a higher prefactor than current known superionic conductors while maintaining a low energy barrier.[29] They attributed the high prefactor to a longer jump distance and higher migration entropy, though they did not characterize the migration entropy directly. The migration entropy are usually derived once other parameters are obtained.[56−58] Direct measurements of migration entropy using first-principles calculations help to better understand its physical origin[59,60] and hence promote new design strategies toward superionic conductors.

Here, we analyzed the prefactor $D_0$ in $Li_3OCl_{1-x}Br_x$ using conventional hopping theory[61]

$$D_0 = \frac{1}{6} f \nu_0 \lambda^2 \exp\left(\frac{\Delta S_m}{k_B}\right) \quad (5)$$

which is governed by correlation factor $f$, true attempt frequency $\nu_0$, jump distance $\lambda$, and the migration entropy $\Delta S_m$. The correlation factor $f$ is treated as one, assuming dilute and isolated mobile-ion carriers.[51] The true attempt frequency represents the oscillator frequency of the moving cation at its lattice sites. The attempt frequency can be approximated by


https://dx.doi.org/10.1021/acsaem.0c02519
ACS Appl. Energy Mater. XXXX, XXX, XXX−XXX

the harmonic potential well expression, although anharmonicity can be present to various degrees in some sytems[56,62]

$$\upsilon_0 = \frac{1}{\lambda}\sqrt{\frac{E_a}{2M_{Li}}} \quad (6)$$

with the mass of Li, $M_{Li}$. The migration entropy can be expressed by the Vineyard formula[63] based on harmonic potential wells and is approximated using only the vibration frequency of the hopping Li ion at the initial and saddle point, I and S, respectively[38,39]

$$\Delta S_m = k_B \ln\left(\frac{\Pi_{i=1}^{3N-1}\nu_i^I}{\Pi_{i=1}^{3N-1}\nu_i^S}\right) \approx k_B \ln\left(\frac{\Pi_1^2\nu^I}{\Pi_1^2\nu^S}\right) \quad (7)$$

Here, we only consider the vibration frequency of the hopping Li ion. This method can provide good approximation results and will not affect our qualitative conclusions.[38,39,64,65]

The calculated attempt frequency, migration entropy, and prefactor in $Li_3OCl_{1-x}Br_x$ are shown in Figure 4. Figure 4a shows that the attempt frequency, calculated by the activation barrier and jump distance, increases with activation energy. We also note that longer jump distances are generally associated with larger activation energy (Figure S7). Figure 4b shows the migration entropy calculated using only the hopping Li-ion vibration frequency. The migration entropy decreases with increasing activation energy, which is interesting since it contradicts the deduction that increasing migration entropy with increasing activation energy is the main cause of the Meyer−Neldel rule.[35] The reason why the migration entropy is negative in $Li_3OCl_{1-x}Br_x$ is straightforward as the saddle site (trigonal plane) is more constrained than the initial site (octahedron), and hence a larger vibration frequency is in the denominator, as shown in eq 7. With increasing activation energy, the migration entropy decreases here due to decreasing initial frequency and increasing saddle frequency (Figure 2b). While we shall note that such kind of correlation between activation energy and migration entropy depends on the local structure of the diffusion path, a more systematic investigation in other common solid electrolytes is needed. Figure 4c shows the jump distance, attempt frequency, and migration entropy of the five structures. These three parameters together lead to a nonlinear variance between prefactor $D_0$, extracted from the Arrhenius plot (Figure 3), and activation energy, as shown in Figure 4d, in contrary to the Meyer−Neldel rule. The trend between prefactor $D_0$ and activation energy obtained in this work is in good agreement with results by Deng et al.[16] (Figure S8). It should be noted that the values of activation energy in Figure 4c,d have discrepancies because Figure 4c is obtained from NEB calculations while Figure 4d is from AIMD calculations but the order is the same. With increasing activation energy, the decreasing migration entropy compensates increasing jump distance and attempt frequency, resulting in a maximum prefactor $D_0$ at $Li_3OCl$ with intermediate activation energy.

In general, a higher migration entropy is preferred for a larger prefactor, which means higher frequency for the mobile Li ion at initial sites and lower frequency at saddle sites (eq 7). Specifically, in $Li_3OCl_{1-x}Br_x$, because the Li-ion vibration frequency increases with the degree of site distortion (Figure 2c,d), more distorted initial sites and less distorted saddle sites are favorable for higher migration entropy (Figure 4a) as well as lower activation energy (Figure 2a). However, considering the other complex factors involving prefactor $D_0$, e.g., the jumping distance and attempt frequency, the variation of prefactor $D_0$ with activation energy may or may not follow the Meyer−Neldel rule ($Li_3OCl_{1-x}Br_x$ disobeys the Meyer−Neldel rule). Thus, a more comprehensive investigation about the vibration, energy landscape, and local structure of the initial and saddle points during the Li-ion migration is needed to understand the correlation between prefactor $D_0$ and activation energy for different types of solid-state electrolytes, which is critical for the optimization of ion diffusivity $D$ at room temperature.

## 4. CONCLUSIONS

In this work, the correlated effect of structural distortion and lattice dynamics on the ionic conductivity was studied in the antiperovskite $Li_3OCl_{1-x}Br_x$. The continuous symmetry measure was applied to evaluate the structural distortion. More distorted initial sites and less distorted saddle sites can lead to a lower energy barrier. Phonon calculations show a softer lattice framework during replacing Cl with more polarizable Br, while the direct cation−anion interactions reflected by the Li-projected phonon band center do not become weaker. The site distortion squeezes the local environment surrounding the Li ion and the structural distortion is found to influence lattice dynamics, especially for the mobile Li ion. In addition, this work analyzed the relationship between the pre-exponential factor and activation energy with respect to the Meyer−Neldel rule. The decreasing migration entropy with increasing activation energy in the antiperovskite $Li_3OCl_{1-x}Br_x$ causes the violation of the rule. We conclude that more distorted initial sites and less distorted saddle sites are beneficial for lower activation energy, and at the same time, higher migration entropy.

## ■ ASSOCIATED CONTENT

### Supporting Information

The Supporting Information is available free of charge at https://pubs.acs.org/doi/10.1021/acsaem.0c02519.

Structural information, NEB results and values of site distortion, phonon DOS, MSD, the correlation between prefactor $D_0$ and activation energy, and generality of the correlation between activation energy and CSM regardless of halide disorder (PDF)

## ■ AUTHOR INFORMATION


### Corresponding Author

**Hong Zhu** − *University of Michigan−Shanghai Jiao Tong University Joint Institute, Shanghai Jiao Tong University, Shanghai 200240, China;* orcid.org/0000-0001-7919-5661; Email: hong.zhu@sjtu.edu.cn

### Authors

**Ronghan Chen** − *University of Michigan−Shanghai Jiao Tong University Joint Institute, Shanghai Jiao Tong University, Shanghai 200240, China*

**Zhenming Xu** − *University of Michigan−Shanghai Jiao Tong University Joint Institute, Shanghai Jiao Tong University, Shanghai 200240, China*

**Yuechuan Lin** − *University of Michigan−Shanghai Jiao Tong University Joint Institute, Shanghai Jiao Tong University, Shanghai 200240, China*




https://dx.doi.org/10.1021/acsaem.0c02519
ACS Appl. Energy Mater. XXXX, XXX, XXX−XXX

**Buyao Lv** − *University of Michigan−Shanghai Jiao Tong University Joint Institute, Shanghai Jiao Tong University, Shanghai 200240, China*

**Shou-Hang Bo** − *University of Michigan−Shanghai Jiao Tong University Joint Institute, Shanghai Jiao Tong University, Shanghai 200240, China;* orcid.org/0000-0001-8963-5261

Complete contact information is available at: https://pubs.acs.org/10.1021/acsaem.0c02519

### Notes

The authors declare no competing financial interest.

## ■ ACKNOWLEDGMENTS

This work was supported by the National Natural Science Foundation of China (51602196, 52072240), the Shanghai Automotive Industry Corporation (1714), and the Materials Genome Initiative Center at Shanghai Jiao Tong University. All simulations were performed at the Shanghai Jiao Tong University High Performance Computing Center.

## ■ REFERENCES

(1) Famprikis, T.; Canepa, P.; Dawson, J. A.; Islam, M. S.; Masquelier, C. Fundamentals of Inorganic Solid-State Electrolytes for Batteries. *Nat. Mater.* **2019**, *18*, 1278−1291.

(2) Li, X.; Liang, J.; Yang, X.; Adair, K. R.; Wang, C.; Zhao, F.; Sun, X. Progress and Perspectives on Halide Lithium Conductors for All-Solid-State Lithium Batteries. *Energy Environ. Sci.* **2020**, *13*, 1429−1461.

(3) Gao, Z.; Sun, H.; Fu, L.; Ye, F.; Zhang, Y.; Luo, W.; Huang, Y. Promises, Challenges, and Recent Progress of Inorganic Solid-State Electrolytes for All-Solid-State Lithium Batteries. *Adv. Mater.* **2018**, *30*, No. 1705702.

(4) Gao, Y.; Nolan, A. M.; Du, P.; Wu, Y.; Yang, C.; Chen, Q.; Mo, Y.; Bo, S. H. Classical and Emerging Characterization Techniques for Investigation of Ion Transport Mechanisms in Crystalline Fast Ionic Conductors. *Chem. Rev.* **2020**, *120*, 5954−6008.

(5) Xiao, Y.; Wang, Y.; Bo, S. H.; Kim, J. C.; Miara, L. J.; Ceder, G. Understanding Interface Stability in Solid-State Batteries. *Nat. Rev. Mater.* **2020**, *5*, 105−126.

(6) Manthiram, A.; Yu, X.; Wang, S. Lithium Battery Chemistries Enabled by Solid-State Electrolytes. *Nat. Rev. Mater.* **2017**, *2*, No. 16103.

(7) Zhao, Q.; Stalin, S.; Zhao, C. Z.; Archer, L. A. Designing Solid-State Electrolytes for Safe, Energy-Dense Batteries. *Nat. Rev. Mater.* **2020**, *5*, 229−252.

(8) Zhang, Z.; Shao, Y.; Lotsch, B.; Hu, Y. S.; Li, H.; Janek, J.; Nazar, L. F.; Nan, C. W.; Maier, J.; Armand, M.; Chen, L. New Horizons for Inorganic Solid State Ion Conductors. *Energy Environ. Sci.* **2018**, *11*, 1945−1976.

(9) Zhao, Y.; Daemen, L. L. Superionic Conductivity in Lithium-Rich Anti-Perovskites. *J. Am. Chem. Soc.* **2012**, *134*, 15042−15047.

(10) Lü, X.; Howard, J. W.; Chen, A.; Zhu, J.; Li, S.; Wu, G.; Dowden, P.; Xu, H.; Zhao, Y.; Jia, Q. Antiperovskite $Li_3OCl$ Superionic Conductor Films for Solid-State Li-Ion Batteries. *Adv. Sci.* **2016**, *3*, No. 1500359.

(11) Zhu, J.; Li, S.; Zhang, Y.; Howard, J. W.; Lü, X.; Li, Y.; Wang, Y.; Kumar, R. S.; Wang, L.; Zhao, Y. Enhanced Ionic Conductivity with $Li_7O_2Br_3$ Phase in $Li_3OBr$ Anti-Perovskite Solid Electrolyte. *Appl. Phys. Lett.* **2016**, *109*, No. 101904.

(12) Emly, A.; Kioupakis, E.; Van Der Ven, A. Phase Stability and Transport Mechanisms in Antiperovskite $Li_3OCl$ and $Li_3OBr$ Superionic Conductors. *Chem. Mater.* **2013**, *25*, 4663−4670.

(13) Kraft, M. A.; Culver, S. P.; Calderon, M.; Böcher, F.; Krauskopf, T.; Senyshyn, A.; Dietrich, C.; Zevalkink, A.; Janek, J.; Zeier, W. G. Influence of Lattice Polarizability on the Ionic Conductivity in the Lithium Superionic Argyrodites $Li_6PS_5X$ (X = Cl, Br, I). *J. Am. Chem. Soc.* **2017**, *139*, 10909−10918.

(14) Muy, S.; Bachman, J. C.; Giordano, L.; Chang, H. H.; Abernathy, D. L.; Bansal, D.; Delaire, O.; Hori, S.; Kanno, R.; Maglia, F.; Lupart, S.; Lamp, P.; Shao-Horn, Y. Tuning Mobility and Stability of Lithium Ion Conductors Based on Lattice Dynamics. *Energy Environ. Sci.* **2018**, *11*, 850−859.

(15) Muy, S.; Voss, J.; Schlem, R.; Koerver, R.; Sedlmaier, S. J.; Maglia, F.; Lamp, P.; Zeier, W. G.; Shao-Horn, Y. High-Throughput Screening of Solid-State Li-Ion Conductors Using Lattice-Dynamics Descriptors. *iScience* **2019**, *16*, 270−282.

(16) Deng, Z.; Radhakrishnan, B.; Ong, S. P. Rational Composition Optimization of the Lithium-Rich $Li_3OCl_{1-x}Br_x$ Anti-Perovskite Superionic Conductors. *Chem. Mater.* **2015**, *27*, 3749−3755.

(17) Kim, K.; Siegel, D. J. Correlating Lattice Distortions, Ion Migration Barriers, and Stability in Solid Electrolytes. *J. Mater. Chem. A* **2019**, *7*, 3216−3227.

(18) Urban, A.; Seo, D. H.; Ceder, G. Computational Understanding of Li-Ion Batteries. *npj Comput. Mater.* **2016**, *2*, No. 16002.

(19) Shi, S.; Gao, J.; Liu, Y.; Zhao, Y.; Wu, Q.; Ju, W.; Ouyang, C.; Xiao, R. Multi-Scale Computation Methods: Their Applications in Lithium-Ion Battery Research and Development. *Chin. Phys. B* **2016**, *25*, No. 018212.

(20) Kresse, G.; Furthmüller, J. Efficient Iterative Schemes for Ab Initio Total-Energy Calculations Using a Plane-Wave Basis Set. *Phys. Rev. B* **1996**, *54*, No. 11169.

(21) Blöchl, P. E. Projector Augmented-Wave Method. *Phys. Rev. B* **1994**, *50*, No. 17953.

(22) Perdew, J. P.; Burke, K.; Ernzerhof, M. Generalized Gradient Approximation Made Simple. *Phys. Rev. Lett.* **1996**, *77*, No. 3865.

(23) Baroni, S.; De Gironcoli, S.; Dal Corso, A.; Giannozzi, P. Phonons and Related Crystal Properties from Density-Functional Perturbation Theory. *Rev. Mod. Phys.* **2001**, *73*, No. 515.

(24) Togo, A.; Tanaka, I. First Principles Phonon Calculations in Materials Science. *Scr. Mater.* **2015**, *108*, 1−5.

(25) Henkelman, G.; Jónsson, H. Improved Tangent Estimate in the Nudged Elastic Band Method for Finding Minimum Energy Paths and Saddle Points. *J. Chem. Phys.* **2000**, *113*, 9978−9985.

(26) Nosé, S. A Unified Formulation of the Constant Temperature Molecular Dynamics Methods. *J. Chem. Phys.* **1984**, *81*, 511−519.

(27) Hoover, W. G. Canonical Dynamics: Equilibrium Phase-Space Distributions. *Phys. Rev. A* **1985**, *31*, No. 1695.

(28) Wu, M.; Xu, B.; Lei, X.; Huang, K.; Ouyang, C. Bulk Properties and Transport Mechanisms of a Solid State Antiperovskite Li-Ion Conductor $Li_3OCl$: Insights from First Principles Calculations. *J. Mater. Chem. A* **2018**, *6*, 1150−1160.

(29) Di Stefano, D.; Miglio, A.; Robeyns, K.; Filinchuk, Y.; Lechartier, M.; Senyshyn, A.; Ishida, H.; Spannenberger, S.; Prutsch, D.; Lunghammer, S.; Rettenwander, D.; Wilkening, M.; Roling, B.; Kato, Y.; Hautier, G. Superionic Diffusion through Frustrated Energy Landscape. *Chem* **2019**, *5*, 2450−2460.

(30) Pinsky, M.; Avnir, D. Continuous Symmetry Measures. 5. The Classical Polyhedra. *Inorg. Chem.* **1998**, *37*, 5575−5582.

(31) Waroquiers, D.; Gonze, X.; Rignanese, G. M.; Welker-Nieuwoudt, C.; Rosowski, F.; Göbel, M.; Schenk, S.; Degelmann, P.; André, R.; Glaum, R.; Hautier, G. Statistical Analysis of Coordination Environments in Oxides. *Chem. Mater.* **2017**, *29*, 8346−8360.

(32) Wakamura, K. Effects of Electronic Band on Activation Energy and of Effective Charge on Lattice Distortion in Superionic Conductors. *J. Phys. Chem. Solids* **1998**, *59*, 591−598.

(33) Francisco, B. E.; Stoldt, C. R.; M'Peko, J. C. Lithium-Ion Trapping from Local Structural Distortions in Sodium Super Ionic Conductor (NASICON) Electrolytes. *Chem. Mater.* **2014**, *26*, 4741−4749.

(34) Harm, S.; Hatz, A. K.; Schneider, C.; Hoefer, C.; Hoch, C.; Lotsch, B. V. Finding the Right Blend: Interplay Between Structure and Sodium Ion Conductivity in the System $Na_5AlS_4$−$Na_4SiS_4$. *Front. Chem.* **2020**, *8*, No. 90.

(35) Krauskopf, T.; Muy, S.; Culver, S. P.; Ohno, S.; Delaire, O.; Shao-Horn, Y.; Zeier, W. G. Comparing the Descriptors for Investigating the Influence of Lattice Dynamics on Ionic Transport Using the Superionic Conductor $Na_3PS_{4-x}Se_x$. *J. Am. Chem. Soc.* **2018**, *140*, 14464−14473.
(36) Schlem, R.; Ghidiu, M.; Culver, S. P.; Hansen, A. L.; Zeier, W. G. Changing the Static and Dynamic Lattice Effects for the Improvement of the Ionic Transport Properties within the Argyrodite $Li_6PS_{5-x}Se_xI$. *ACS Appl. Energy Mater.* **2020**, *3*, 9−18.
(37) Krauskopf, T.; Culver, S. P.; Zeier, W. G. Bottleneck of Diffusion and Inductive Effects in $Li_{10}Ge_{1-x}Sn_xP_2S_{12}$. *Chem. Mater.* **2018**, *30*, 1791−1798.
(38) Wu, H.; Mayeshiba, T.; Morgan, D. High-Throughput Ab-Initio Dilute Solute Diffusion Database. *Sci. Data* **2016**, *3*, No. 160054.
(39) Lu, H. J.; Wu, H.; Zou, N.; Lu, X. G.; He, Y. L.; Morgan, D. First-Principles Investigation on Diffusion Mechanism of Alloying Elements in Dilute Zr Alloys. *Acta Mater.* **2018**, *154*, 161−171.
(40) Smith, J. G.; Siegel, D. J. Low-Temperature Paddlewheel Effect in Glassy Solid Electrolytes. *Nat. Commun.* **2020**, *11*, No. 1483.
(41) Jansen, M. Volume Effect or Paddle-Wheel Mechanism - Fast Alkali-Metal Ionic Conduction in Solids with Rotationally Disordered Complex Anions. *Angew. Chem., Int. Ed.* **1991**, *30*, 1547−1558.
(42) Zhao, Q.; Pan, L.; Li, Y. J.; Chen, L. Q.; Shi, S. Q. Rotational Motion of Polyanion versus Volume Effect Associated with Ionic Conductivity of Several Solid Electrolytes. *Rare Met.* **2018**, *37*, 497−503.
(43) Culver, S. P.; Koerver, R.; Krauskopf, T.; Zeier, W. G. Designing Ionic Conductors: The Interplay between Structural Phenomena and Interfaces in Thiophosphate-Based Solid-State Batteries. *Chem. Mater.* **2018**, *30*, 4179−4192.
(44) Bernges, T.; Culver, S. P.; Minafra, N.; Koerver, R.; Zeier, W. G. Competing Structural Influences in the Li Superionic Conducting Argyrodites $Li_6PS_{5-x}Se_xBr$ $(0 \leq x \leq 1)$ upon Se Substitution. *Inorg. Chem.* **2018**, *57*, 13920−13928.
(45) He, X.; Zhu, Y.; Epstein, A.; Mo, Y. Statistical Variances of Diffusional Properties from Ab Initio Molecular Dynamics Simulations. *npj Comput. Mater.* **2018**, *4*, No. 18.
(46) Meyer, W.; Neldel, H. Relation between the Energy Constant and the Quantity Constant in the Conductivity−Temperature Formula of Oxide Semiconductors. *Z. Tech. Phys.* **1937**, *18*, 588.
(47) Yelon, A.; Movaghar, B.; Branz, H. M. Origin and Consequences of the Compensation (Meyer-Neldel) Law. *Phys. Rev. B* **1992**, *46*, No. 12244.
(48) Almond, D. P.; West, A. R. Entropy Effects in Ionic Conductivity. *Solid State Ionics* **1986**, *18*−*19*, 1105−1109.
(49) Muy, S.; Bachman, J. C.; Chang, H. H.; Giordano, L.; Maglia, F.; Lupart, S.; Lamp, P.; Zeier, W. G.; Shao-Horn, Y. Lithium Conductivity and Meyer-Neldel Rule in $Li_3PO_4$-$Li_3VO_4$-$Li_4GeO_4$ Lithium Superionic Conductors. *Chem. Mater.* **2018**, *30*, 5573−5582.
(50) Šedivý, L.; Belas, E.; Grill, R.; Musiienko, A.; Vasylchenko, I. Extension of Meyer-Neldel Rule Using Chemical Diffusion Experiments in CdTe. *J. Alloys Compd.* **2019**, *788*, 897−904.
(51) Marcolongo, A.; Marzari, N. Ionic Correlations and Failure of Nernst-Einstein Relation in Solid-State Electrolytes. *Phys. Rev. Mater.* **2017**, *1*, No. 025402.
(52) Ram, S. K.; Kumar, S.; Roca i Cabarrocas, P. Normal and Anti Meyer-Neldel Rule in Conductivity of Highly Crystallized Undoped Microcrystalline Silicon Films. *J. Non-Cryst. Solids* **2008**, *354*, 2263−2267.
(53) Ngai, K. L. Meyer-Neldel Rule and Anti Meyer-Neldel Rule of Ionic Conductivity Conclusions from the Coupling Model. *Solid State Ionics* **1998**, *105*, 231−235.
(54) Kaup, K.; Bazak, J. D.; Vajargah, S. H.; Wu, X.; Kulisch, J.; Goward, G. R.; Nazar, L. F. A Lithium Oxythioborosilicate Solid Electrolyte Glass with Superionic Conductivity. *Adv. Energy Mater.* **2020**, *10*, No. 1902783.
(55) Nowick, A. S.; Lee, W. K.; Jain, H. Survey and Interpretation of Pre-Exponentials of Conductivity. *Solid State Ionics* **1988**, *28*−*30*, 89−94.
(56) Almond, D. P.; West, A. R. The Activation Entropy for Transport in Ionic Conductors. *Solid State Ionics* **1987**, *23*, 27−35.
(57) Varotsos, P.; Alexopoulos, K. Estimation of the Migration Enthalpy and Entropy for Cation Vacancy Motion in Alkali Halides with the NaCl-Type Structure. *Phys. Rev. B* **1977**, *15*, No. 2348.
(58) Dobson, T. W.; Wager, J. F.; Van Vechten, J. A. Entropy of Migration for Atomic Hopping. *Phys. Rev. B* **1989**, *40*, No. 2962.
(59) Toyoura, K.; Koyama, Y.; Kuwabara, A.; Oba, F.; Tanaka, I. First-Principles Approach to Chemical Diffusion of Lithium Atoms in a Graphite Intercalation Compound. *Phys. Rev. B* **2008**, *78*, No. 214303.
(60) Koettgen, J.; Schmidt, P. C.; Bučko, T.; Martin, M. Ab Initio Calculation of the Migration Free Energy of Oxygen Diffusion in Pure and Samarium-Doped Ceria. *Phys. Rev. B* **2018**, *97*, No. 024305.
(61) Mehrer, H. Diffusion in Solids—Fundamentals, Methods, Materials, Diffusion-Controlled Processes. In *Springer Series in Solid-State Sciences*; Springer, 2007.
(62) Wert, C.; Zener, C. Interstitial Atomic Diffusion Coefficients. *Phys. Rev.* **1949**, *76*, No. 1169.
(63) Vineyard, G. H. Frequency Factors and Isotope Effects in Solid State Rate Processes. *J. Phys. Chem. Solids* **1957**, *3*, 121−127.
(64) Legrain, F.; Carrete, J.; Van Roekeghem, A.; Curtarolo, S.; Mingo, N. How Chemical Composition Alone Can Predict Vibrational Free Energies and Entropies of Solids. *Chem. Mater.* **2017**, *29*, 6220−6227.
(65) Koettgen, J.; Martin, M. The Effect of Jump Attempt Frequencies on the Ionic Conductivity of Doped Ceria. *J. Phys. Chem. C* **2019**, *123*, 19437−19446.


https://dx.doi.org/10.1021/acsaem.0c02519
*ACS Appl. Energy Mater.* XXXX, XXX, XXX−XXX